

PCCP

Accepted Manuscript



This is an *Accepted Manuscript*, which has been through the Royal Society of Chemistry peer review process and has been accepted for publication.

Accepted Manuscripts are published online shortly after acceptance, before technical editing, formatting and proof reading. Using this free service, authors can make their results available to the community, in citable form, before we publish the edited article. We will replace this *Accepted Manuscript* with the edited and formatted *Advance Article* as soon as it is available.

You can find more information about *Accepted Manuscripts* in the [Information for Authors](#).

Please note that technical editing may introduce minor changes to the text and/or graphics, which may alter content. The journal's standard [Terms & Conditions](#) and the [Ethical guidelines](#) still apply. In no event shall the Royal Society of Chemistry be held responsible for any errors or omissions in this *Accepted Manuscript* or any consequences arising from the use of any information it contains.

Direct measurements of the total rate constant of the reaction $\text{NCN} + \text{H}$ and implications for the product branching ratio and the enthalpy of formation of NCN

Nancy Faßheber, Johannes Dammeier, and Gernot Friedrichs*

Received Xth XXXXXXXXXXXX 20XX, Accepted Xth XXXXXXXXXXXX 20XX

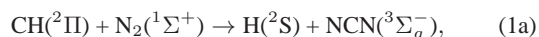
First published on the web Xth XXXXXXXXXXXX 200X

DOI: 10.1039/b000000x

The overall rate constant of the reaction (2), $\text{NCN} + \text{H}$, which plays a key role in prompt-NO formation in flames, has been directly measured at temperatures $962 \text{ K} < T < 2425 \text{ K}$ behind shock waves. NCN radicals and H atoms were generated by the thermal decomposition of NCN_3 and $\text{C}_2\text{H}_5\text{I}$, respectively. NCN concentration-time profiles were measured by sensitive narrow-line-width laser absorption at a wavelength of $\lambda = 329.1302 \text{ nm}$. The obtained rate constants are best represented by the combination of two Arrhenius expressions, $k_2/(\text{cm}^3 \text{mol}^{-1} \text{s}^{-1}) = 3.49 \times 10^{14} \exp(-33.3 \text{ kJ mol}^{-1}/RT) + 1.07 \times 10^{13} \exp(+10.0 \text{ kJ mol}^{-1}/RT)$, with a small uncertainty of $\pm 20\%$ at $T = 1600 \text{ K}$ and $\pm 30\%$ at the upper and lower experimental temperature limits. The two Arrhenius terms basically can be attributed to the contributions of reaction channel (2a) yielding $\text{CH} + \text{N}_2$ and channel (2b) yielding $\text{HCN} + \text{N}$ as the products. A more refined analysis taking into account experimental and theoretical literature data provided a consistent rate constant set for k_{2a} , its reverse reaction k_{1a} ($\text{CH} + \text{N}_2 \rightarrow \text{NCN} + \text{H}$), k_{2b} , as well as a value for the controversial enthalpy of formation of NCN , $\Delta_f H_{298 \text{ K}}^\circ = 450 \text{ kJ/mol}$. The analysis verifies the expected strong temperature dependence of the branching fraction $\phi = k_{2b}/k_2$ with reaction channel (2b) dominating at the experimental high-temperature limit. In contrast, reaction (2a) dominates at the low-temperature limit with a possible minor contribution of the HNCN forming recombination channel (2d) at $T < 1150 \text{ K}$.

1 Introduction

Nitrogen oxides, NO and NO_2 (NO_x), are major atmospheric pollutants formed by different reaction mechanisms in combustion processes. Especially under fuel rich combustion conditions, the so-called prompt-NO formation pathway becomes significant. According to Fenimore,¹ prompt-NO formation is initiated by the reaction of small hydrocarbon radicals with molecular nitrogen from the combustion air. Although it has been proven both theoretically^{2–4} and experimentally^{5,6} that the key initiation reaction $\text{CH} + \text{N}_2$ yields the spin-allowed products $\text{H} + \text{NCN}$,



instead of the previously assumed spin-forbidden products $\text{N} + \text{HCN}$,



so far NCN chemistry has only been implemented in two detailed kinetic mechanisms for combustion modeling, namely konnov0-6 and GDFkin3.0_NCNCN.^{7,8} Adopted NCN reaction rate constant parameters are largely based on the theoretical work of the M. C. Lin group who reported rate constant values for the most important bimolecular NCN consumption reactions $\text{NCN} + \text{H}$,^{2,4} O ,⁹ OH ,¹⁰ and others.^{11–13} Experimental high-temperature data for

NCN reactions are scarce. Next to the early shock tube detection of NCN and indirect rate constant measurements of the reaction $\text{NCN} + \text{H}$ performed by Vasudevan et al.,⁶ Busch and Olzmann investigated the thermal decomposition of NCN by means of C-ARAS detection behind shock waves.^{14,15} All other direct high-temperature measurements are based on work performed in the Kiel shock tube laboratory operated by us. We use the thermal decomposition of cyanogen azide (NCN_3) as a quantitative source of NCN radicals.¹⁶ So far, we were able to report rate constant data for the bimolecular NCN reactions with O , NCN , NO , NO_2 , and its unimolecular decomposition $\text{NCN} + \text{M} \rightarrow \text{C} + \text{N}_2 + \text{M}$.^{17,18} The purpose of this paper is to provide the first direct high-temperature measurements of the total rate constant of the reaction $\text{NCN} + \text{H}$. At combustion temperatures, the reaction exhibits two main reaction channels:



Depending on the reaction conditions, two additional minor reaction channels forming $\text{HNC} + \text{N}$ and HNCN are accessible (see discussion section). The rate of reaction (2) and its exact branching ratio turned out to be crucial factors for modelling the fate of NCN in hydrocarbon flames.^{7,8,19} On the one hand reaction (2a) constitutes the reverse of the prompt-NO initiation reaction (1a) and can be calculated from k_{1a} via the thermochemical equilibrium constant $K(\text{CH} + \text{N}_2 \rightleftharpoons \text{NCN} + \text{H}) = k_{1a}/k_{2a}$. On the other hand the products of reaction (2b) are the same as the products of the formerly assumed spin-forbidden reaction (1b), which brings the new NCN chemistry back to the old Fenimore NO_x formation route.

Institut für Physikalische Chemie, Christian-Albrechts-Universität zu Kiel, Max-Eyth-Str. 1, 24118 Kiel, Germany.
E-mail: friedrichs@phc.uni-kiel.de; Tel: +49 431 880 7742; Fax: +49 880 7743

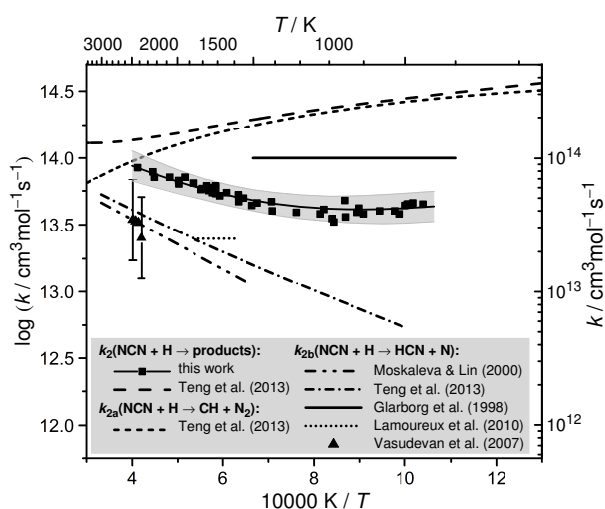


Fig. 1 Experimental and theoretical literature rate constant data for the reaction $\text{NCN} + \text{H}$ in comparison with the results of this work. Estimate of Glarborg et al.²⁰, shock tube data of Vasudevan et al.⁶, flame data of Lamoureux et al.,⁸ and theoretical predictions of Teng et al.⁴ and Moskaleva and Lin² are illustrated as outlined in the legend. The squares depict the experimental data of this work; the shaded area and the thick solid curve correspond to the range of uncertainty and a fit of the experimental data, respectively.

Reported rate constant values for reaction $\text{NCN} + \text{H}$ have been included in the Arrhenius diagram shown in Fig. 1. An early rate constant estimate of Glarborg et al.²⁰ assumed reaction (2b) to proceed with a temperature independent rate constant close to the collisional rate, $k_{2b} = 1 \times 10^{14} \text{ cm}^3 \text{ mol}^{-1} \text{ s}^{-1}$ (upper solid line). Shortly after, the reaction $\text{NCN} + \text{H}$ has been theoretically analyzed by Moskaleva and Lin.² As a side note in their paper on the overall rate constant of the reaction $\text{CH} + \text{N}_2 \rightarrow \text{NCN} + \text{H}$, but unfortunately without giving much details on the underlying theoretical model, they reported a pressure independent rate constant expression of $k_{2b} = 1.89 \times 10^{14} \times \exp(-35.3 \text{ kJ/mol}/RT) \text{ cm}^3 \text{ mol}^{-1} \text{ s}^{-1}$ revealing that the reaction takes place over a sizable barrier (lower dash-dotted line). Hence, with $k_{2b} = 1.1 \times 10^{13} \text{ cm}^3 \text{ mol}^{-1} \text{ s}^{-1}$ at $T = 1500 \text{ K}$, the reaction is one order of magnitude slower than the initial estimate. Experimentally, Vasudevan et al.⁶ indirectly determined the rate constant of reaction (2b) in the temperature range of $2378 \text{ K} < T < 2492 \text{ K}$ by measuring absorption-time profiles of NCN in ethane/ N_2 mixtures behind shock waves (triangles with error bars). Following fast NCN generation by reaction (1a), the observed slow decays of the NCN radical concentration profiles were found to be consistent with k_{2b} values close to the ones reported by Moskaleva and Lin.

In an indirect experimental and numerical study of the role of NCN formation in low pressure flames, Lamoureux et al.⁸ reported the value $k_{2b} = 2.5 \times 10^{13} \text{ cm}^3 \text{ mol}^{-1} \text{ s}^{-1}$ (dotted line), which was also adopted for the GDFkin3.0_NCN mechanism. Essentially, this value had been chosen to match the experimentally measured NCN and NO concentration profiles in methane

and acetylene flames with peak flame temperatures of $T = 1600 \text{ K} - 1835 \text{ K}$. Therefore, this reported value is highly dependent on the value of the assumed absorption cross section for NCN, which is subject to ongoing discussion.²¹ Furthermore, the assumed enthalpy of formation of NCN, here $\Delta_f H_{298 \text{ K}}^\circ = 452 \text{ kJ/mol}$, is a critical quantity as k_{2a} is calculated from k_{1a} via thermochemical equilibrium in their simulations. The crucial role of NCN thermochemistry for modelling prompt-NO formation in flames has been recently highlighted in a paper by Goos et al.²² They nicely demonstrated that the modelled branching ratio of the overall reaction (2) heavily depends on the assumed enthalpy of formation value for NCN. For example, by switching the enthalpy of formation from the low value $\Delta_f H_{298 \text{ K}}^\circ = 444.5 \text{ kJ/mol}$ (representative for theoretical estimates based on single-reference computations)^{16,23} to the high value 466.5 kJ/mol (experimental result based on photodissociation experiments)²⁴ both the simulated NCN peak mole fraction and final NO yield varied by a factor of about 3 for a fuel rich low-pressure $\text{CH}_4\text{-O}_2\text{-N}_2$ flame. In view of this large variation it becomes clear that also the indirect k_{2b} value of Lamoureux et al. is uncertain.

Very recently the M.C. Lin group⁴ updated their theoretical prediction of the rate constants of the reactions $\text{CH} + \text{N}_2$ and $\text{NCN} + \text{H}$ based on (i) high-level *ab initio* calculation (CCSD(T) with complete basis set limit) of the underlying quartet and doublet potential energy surfaces and (ii) by correcting a previous coding error in a program used in their original paper² from the year 2000. Teng et al.⁴ clearly showed that reaction (2b) is a spin-allowed process predominantly taking place on a quartet surface, in contrast to reaction (2a) taking place only on a doublet surface. In comparison with their previous work, they now recommend the rate expression $k_{2b} = 4.96 \times 10^{12} \times T^{0.41} \times \exp(-22.8 \text{ kJ/mol}/RT) \text{ cm}^3 \text{ mol}^{-1} \text{ s}^{-1}$ yielding 20% to 40% higher k_{2b} values at temperatures from 1500 K to 2000 K (upper dash-dotted line in Fig. 1). Another important finding was that an alternative reaction channel yielding $\text{HNC} + \text{N}$ is minor and that the recombination reaction yielding HNCN , which dominates at room temperature, contributes to less than 5% at combustion relevant temperatures of $T > 1000 \text{ K}$ at 1 bar total pressure. Remarkably high total rate constant values with a shallow minimum of $k_2 \approx 1.3 \times 10^{14} \text{ cm}^3 \text{ mol}^{-1} \text{ s}^{-1}$ at $T = 3180 \text{ K}$ have been reported in their work as well (long-dashed curve), which we consider unfeasible. As it turns out in this work, the recommendation of Teng et al. for reaction channel (2a) alone is already up to 6 times higher (short-dashed curve) than our experimentally determined total rate constant k_2 (see also Discussion Section 4).

From this short overview of existing literature data we conclude that a reliable modeling of NCN chemistry in flames is not possible so far. Clearly, experimental data on the rate constant of the reaction $\text{NCN} + \text{H}$ are needed to constrain the rate constant uncertainties and to advance current prompt-NO formation models.

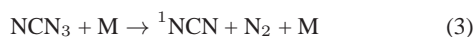
2 Experimental

Shock tube apparatus

All experiments were carried out in an electropolished stainless steel shock tube with inner diameter of 81 mm. A more detailed description can be found elsewhere.²⁵ Briefly, hydrogen or mixtures of hydrogen and nitrogen were used as driver gas; diaphragms were made from 80 or 100 μm thick aluminium foil. The experimental conditions behind the incident and reflected shock waves were calculated from pre-shock conditions and the shock wave velocity, which was measured by four fast piezo-electric sensors (PCB Piezotronics M113A21). A frozen-chemistry code was applied taking into account real gas effects and the measured shock wave damping, which was on the order of 1% per meter. Storage gas mixtures of 500-750 ppm NCN_3 and 1000 ppm $\text{C}_2\text{H}_5\text{I}$ in argon were prepared using the partial pressure method and were further diluted with argon using calibrated mass flow controllers (Aera, FC-7700CU). The low pressure section of the shock tube was flushed for about 5 min at $p \approx 30$ mbar to reduce possible adsorption effects on the shock tube wall.

NCN precursor

The thermal decomposition of cyanogen azide (NCN_3)



has been used as a quantitative source of NCN radicals.^{26,27} It was shown in previous publications^{16,28} that the thermal decomposition initially yields NCN in its first electronically excited singlet state. Under the experimental conditions applied in this work with total densities $\rho > 2 \times 10^{-6}$ mol/cm³ and temperatures $T > 962$ K, the subsequent collision induced intersystem crossing (CIISC) is rate limiting for triplet NCN formation according to



The CIISC efficiency is strongly dependent on the nature of the collider, reveals a non-linear pressure dependence due to a pressure saturation effect, and increases with increasing temperature.^{18,28} In order to accurately model the initial formation rate of ${}^3\text{NCN}$ (denoted NCN in the following), the CIISC rate constant has been allowed to vary within the error limit reported by Dammeier et al.²⁸

The highly toxic and explosive precursor molecule NCN_3 has been directly synthesized using a procedure described previously.^{29,30} Briefly, a small amount of gaseous cyanogen bromide (BrCN , ~ 20 mbar) was passed into an evacuated 1 L glass flask containing a huge excess of solid sodium azide (NaN_3). After a 8 - 10 h reaction time, the gaseous products were analyzed by FTIR spectroscopy. Almost no water and carbon dioxide ($\sim 0.01\%$), which serves as an indicator for a potential gas leak, were present in the reaction samples and the impurities of remaining cyanogen bromide were well below 4%, in some cases $< 0.1\%$. A slow decomposition of about 10% NCN_3 per day took place in the storage flask, therefore mixtures were used up within 3 days. Accurate initial NCN_3 mole fraction in the actual reaction mixtures were determined by modeling the maximum NCN yield in the

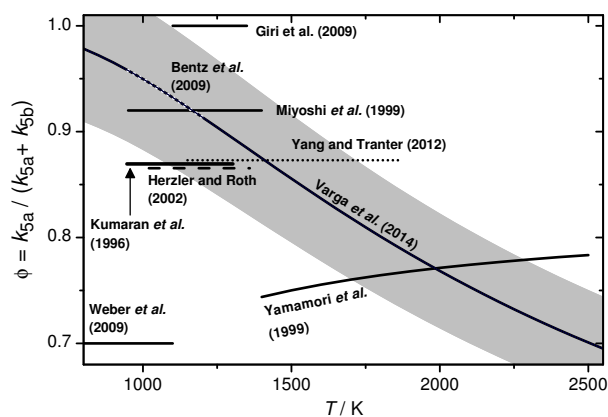


Fig. 2 Selected literature values for the branching ratio ϕ of the thermal decomposition of ethyl iodide yielding $\text{C}_2\text{H}_5 + \text{I}$ (channel 5a) and $\text{C}_2\text{H}_4 + \text{HI}$ (channel 5b), respectively. H and/or I atom resonance absorption measurements: Kumaran et al.,³¹ Yamamori et al.,³² Miyoshi et al.,³³ Herzler and Roth,³⁴ Giri et al.,³⁵ and Bentz et al.,³⁶ laser schlieren technique: Yang and Tranter;³⁷ mass spectrometry: Weber et al.,³⁸ global optimization: Varga et al.³⁹ The gray area represents the assumed uncertainty range of $\pm 7\%$.

experiments and were found to be consistent with the expected NCN_3 content in the storage gas mixtures in all cases.

H precursor

Hydrogen atoms were generated by the thermal unimolecular decomposition of ethyl iodide ($\text{C}_2\text{H}_5\text{I}$). Under typical experimental conditions behind shock waves, the reaction can be assumed to take place close to the high pressure limit³⁹ and exhibits two main reaction channels:



H atom formation proceeds through the fast subsequent decomposition of the ethyl radical,



Although ethyl iodide has been widely used as an H atom precursor, until recently the assumed absolute values and temperature dependences of the H atom yield were uncertain and often represented the most significant source of error in such studies. Selected values of reported branching ratios $\phi = k_{5a}/(k_{5a} + k_{5b})$ are collected in Fig. 2. The most frequently used value of $\phi = 0.87 \pm 0.11$ is based on direct H and I atom resonance absorption spectroscopic (ARAS) measurements performed by Kumaran et al.³¹ at temperatures of $946 \text{ K} < T < 1303 \text{ K}$. Also based on ARAS experiments, Herzler and Roth³⁴ reported a coinciding value, Yamamori et al.³² used lower values of $\phi < 0.78$ at overall higher temperatures, Miyoshi et al.³³ determined a higher value of $\phi = (0.92 \pm 0.06)$, and Giri et al.³⁵ assumed $\phi = 1$ by considering the hydrogen forming pathway only. Recently,

Weber et al.,³⁸ Yang and Tranter,³⁷ and Bentz et al.³⁶ revisited the ethyl iodide pyrolysis. Whereas Yang and Tranter found excellent agreement with their laser-schlieren densitometry shock tube measurements by assuming $\phi = 0.87$, Weber et al. report a significantly lower value of $\phi = (0.7 \pm 0.1)$ from a mass spectrometric investigation of the flash pyrolysis of ethyl iodide. However, Bentz et al. could show by a combination of H- and I-ARAS measurements and statistical rate calculations that the abstraction reaction $\text{H} + \text{C}_2\text{H}_5\text{I} \rightarrow \text{C}_2\text{H}_5 + \text{HI}$, which had been neglected in former studies, needs to be taken into account for an accurate analysis of the branching ratio. Their experimental data, together with other available literature data, have been very recently reanalyzed by Varga et al.³⁹ in a follow-up publication using a new global optimization method developed by Turányi.⁴⁰ The simultaneous optimization of the rate constant expressions of all relevant reactions yielded a considerably temperature dependent branching ratio decreasing from $\phi(T = 962 \text{ K}) = 0.96$ to $\phi(T = 2450 \text{ K}) = 0.71$ over the temperature range of this study. A very low 3σ uncertainty level of ± 0.035 has been specified by Varga et al. at a temperature of $T = 1200 \text{ K}$. As can be seen in Fig. 2 the recommended branching ratios are consistent with most of the previous literature data. We consider these results to be most reliable and therefore adopted the ethyl iodide decomposition mechanism as reported by Varga et al. It is included in the list of reactions in Table 1.

We have recommended the use of a different expression with opposite temperature dependence of ϕ in a previous paper dating back to the year 2002.⁴¹ That recommendation was based on a theoretical treatment of the unimolecular decomposition of ethyl iodide with barrier heights taken from the paper of Kumaran et al. Then, the energy barrier E_0 of the I atom forming C-I bond fission channel (5a) was assumed to be about 15 kJ/mol higher than of the HI elimination channel (5b). However, the recent accurate CCSD(T) ab initio data of Bentz et al.³⁶ showed that both barriers are more or less energetically equal, which is more consistent with the reported decrease of ϕ with increasing temperature. For a more detailed treatment of the unimolecular decomposition reactions of alkyl iodides in the framework of statistical rate theories we refer to the work of Kumaran et al., Miyoshi et al., and Bentz et al.^{31,33,36}

NCN detection

Triplet NCN radicals were detected by time-resolved difference amplification laser absorption spectroscopy at $\tilde{\nu} = 30383.11 \text{ cm}^{-1}$ ($\lambda = 329.1302 \text{ nm}$). The absorption feature at this wavelength mainly stems from a superposition of the $^3\Pi_1$ sub band of the $\tilde{A}^3\Pi_u(000) - \tilde{X}^3\Sigma_g(000)$ and the Q_1 band head of the $^3\Sigma^+(010) - ^3\Pi(010)$ transition.²¹ About 1 mW UV laser radiation was generated by intra-cavity frequency doubling of a continuous-wave ring-dye laser (Coherent, 899) with DCM-Special as dye pumped with a solid state Nd:YVO₄ laser using 8 W at $\lambda = 532 \text{ nm}$ (Coherent Verdi V10). The wavelength of the laser fundamental was measured interferometrically by a wavemeter (MetroLux) with an accuracy of $\Delta\tilde{\nu} \approx \pm 0.015 \text{ cm}^{-1}$. The UV laser beam was split into a detection and a reference beam by a (50:50) beam splitter plate. The detection beam was passed through the shock

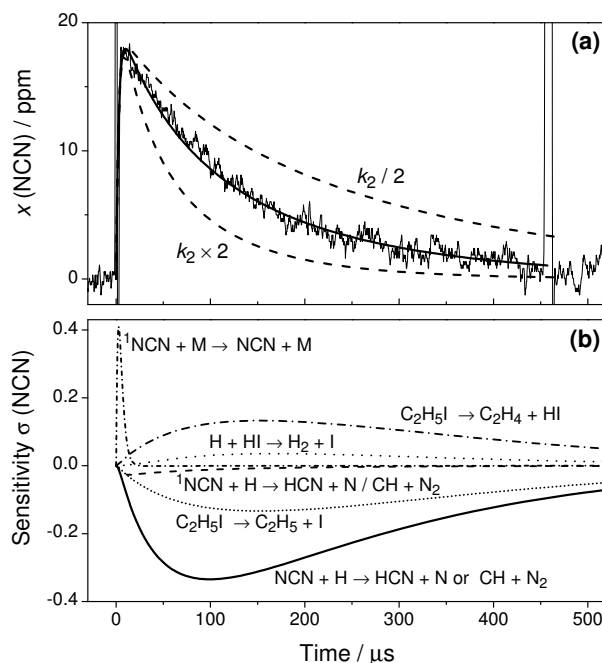


Fig. 3 (a) Experimental NCN profile in comparison with numerical simulations. $T = 1720 \text{ K}$, $\rho = 3.43 \times 10^{-6} \text{ mol/cm}^3$, $p = 490 \text{ mbar}$, $x(\text{NCN}_3) = 21 \text{ ppm}$, $x(\text{C}_2\text{H}_5\text{I}) = 72 \text{ ppm}$, $k_2 = 5.5 \times 10^{13} \text{ cm}^3 \text{ mol}^{-1} \text{ s}^{-1}$. (b) Sensitivity analysis.

tube and coupled into an optical fiber (Thorlabs BF H22-550) connected to a balanced photodetector and amplifier (Thorlabs PDB 150A-EC). The intensity of the reference laser beam was fine-tuned by a variable neutral density filter to match the intensity of the detection beam. The resulting difference signals were low-pass-filtered (1.4 MHz), amplified (Ortec Fast Preamp 9305, 18 dB), and stored by an analog input board (Measurement Computing, PCI-DAS4020/12, 20 MHz, 12 bit). The NCN concentration-time profiles were calculated from the detected absorption profiles based on NCN absorption cross sections $\log(\sigma(\text{base e})/(\text{cm}^2 \text{ mol}^{-1})) = 8.9 - 8.3 \times 10^{-4} \times T/\text{K}$ previously measured with an accuracy of $\pm 25\%$ using the same apparatus at similar temperatures and pressures.¹⁶

3 Results

The reaction of NCN radicals with hydrogen atoms has been investigated behind incident and reflected shock waves in the temperature and pressure ranges $962 \text{ K} < T < 2425 \text{ K}$ and $290 \text{ mbar} < p < 2130 \text{ mbar}$, respectively, at three different total densities of $\rho \approx 3.5 \times 10^{-6}$, 7.4×10^{-6} , and $1.5 \times 10^{-5} \text{ mol/cm}^3$. Reaction gas mixtures contained 72-363 ppm ethyl iodide and 3-31 ppm NCN₃ in argon. In most cases, a large excess of ethyl iodide with $[\text{C}_2\text{H}_5\text{I}]_0/[\text{NCN}_3]_0$ ratios up to 60 was applied, hence the hydrogen atom was used as the excess species. Experimental conditions are listed in Table 2.

Fig. 3a illustrates a typical experiment behind the incident shock wave at a temperature $T = 1720 \text{ K}$ and a total density $\rho =$

Table 1 Rate constant parameters for important NCN reactions and the ethyl iodide submechanism. Rate constants are given in terms of $k = AT^n \exp(-E_a/RT)$ in units of $\text{cm}^3, \text{mol}^{-1}, \text{s}^{-1}$ and kJ. The listed rate constants for NCN (representing ^3NCN) reactions have been duplicated for ^1NCN to approximately take into account ^1NCN secondary chemistry. In addition to the reactions listed here, the GRI-Mech 3.0 has been used as base mechanism⁴² supplemented by iodine chemistry adopted from our previous work.⁴³

No.	Reaction	A	n	E_a	Ref.
3	$\text{NCN}_3 \rightleftharpoons ^1\text{NCN} + \text{N}_2$	4.9×10^9		71	28
4	$^1\text{NCN} \rightarrow \text{NCN}$	2.0×10^6		31	28
2	$\text{NCN} + \text{H} \rightarrow \text{products}$				see text
2a	$\text{NCN} + \text{H} \rightleftharpoons \text{CH} + \text{N}_2$	4.2×10^{15}	-0.69	2.0	this work ^b
2b	$\text{NCN} + \text{H} \rightleftharpoons \text{HCN} + \text{N}$	7.9×10^{12}	0.41	22.8	this work ^a
7	$\text{NCN} + \text{M} \rightleftharpoons \text{C} + \text{N}_2 + \text{M}$	8.9×10^{14}		260	17
8	$\text{NCN} + \text{NCN} \rightleftharpoons \text{CN} + \text{CN} + \text{N}_2$	3.7×10^{12}			28
9	$\text{NCN} + \text{C} \rightleftharpoons \text{CN} + \text{CN}$	1.0×10^{14}			28
10	$\text{NCN} + \text{N} \rightleftharpoons \text{N}_2 + \text{CN}$	1.0×10^{13}			2
11	$\text{NCN} + \text{CN} \rightleftharpoons \text{C}_2\text{N}_2 + \text{N}$	1.3×10^{14}		33.5	2
11	$\text{NCN} + \text{CH} \rightleftharpoons \text{HCN} + \text{CN}$	3.2×10^{13}		-3.6	2
13	$\text{NCN} + \text{CH}_2 \rightleftharpoons \text{H}_2\text{CN} + \text{CN}$	8.0×10^{13}		26.9	2
5a	$\text{C}_2\text{H}_5\text{I} \rightleftharpoons \text{C}_2\text{H}_5 + \text{I}$	3.4×10^{13}		203	39
5b	$\text{C}_2\text{H}_5\text{I} \rightleftharpoons \text{C}_2\text{H}_4 + \text{HI}$	4.7×10^{13}		226	39
6	$\text{C}_2\text{H}_5 + \text{M} \rightleftharpoons \text{C}_2\text{H}_4 + \text{H} + \text{M}$	1.0×10^{18}		140	39
14	$\text{C}_2\text{H}_5\text{I} + \text{H} \rightleftharpoons \text{C}_2\text{H}_5 + \text{HI}$	1.0×10^{15}		21.6	39
15	$\text{C}_2\text{H}_5\text{I} + \text{I} \rightleftharpoons \text{C}_2\text{H}_5 + \text{I}_2$	4.0×10^{13}		69.9	44
16a	$\text{C}_2\text{H}_5 + \text{H} \rightleftharpoons \text{CH}_3 + \text{CH}_3$	4.2×10^{13}			45
16b	$\text{C}_2\text{H}_5 + \text{H} \rightleftharpoons \text{C}_2\text{H}_4 + \text{H}_2$	1.2×10^{12}			46
17	$\text{H} + \text{HI} \rightleftharpoons \text{H}_2 + \text{I}$	6.6×10^{13}		4.1	39

^a Rate expression of Teng et al.⁴ scaled by a factor of 1.6.

^b Assuming $\Delta_f H_{298\text{K}}^\circ(\text{NCN}) = 450 \text{ kJ/mol}$; this corresponds to $k_{1a}(\text{CH} + \text{N}_2 \rightarrow \text{NCN} + \text{H}) = 2.3 \times 10^{10} \times T^{0.53} \times \exp(-71.2 \text{ kJ/mol}/RT)$.

Table 2 Experimental conditions and results.

T/K	$\rho \times 10^6 / \text{mol cm}^{-3}$	$x(\text{NCN}_3)$ ppm	$x(\text{C}_2\text{H}_5\text{I})$ ppm	$k_2 \times 10^{-13} / \text{cm}^3 \text{mol}^{-1} \text{s}^{-1}$	T/K	$\rho \times 10^6 / \text{mol cm}^{-3}$	$x(\text{NCN}_3)$ ppm	$x(\text{C}_2\text{H}_5\text{I})$ ppm	$k_2 \times 10^{-13} / \text{cm}^3 \text{mol}^{-1} \text{s}^{-1}$
1186	3.78	7.4	75	3.3	962	3.52	3.8	185	4.5
1714	3.43	19.0	72	6.1	1000	3.57	4.0	185	4.4
1720	3.43	21.0	72	5.5	1192	3.77	4.6	185	3.5
1813	3.46	21.8	72	5.8	1230	3.80	5.2	185	3.8
1870	3.46	22.8	72	6.5	1552	4.03	9.5	185	5.0
1936	4.20	9.0	76	7.2	1747	3.44	27.5	184	6.0
1991	3.51	27.8	72	6.8					
2070	3.54	23.5	72	7.2	1482	3.99	5.0	299	4.6
2227	3.57	25.0	72	7.2	1509	4.01	3.0	104	4.4
2242	3.55	26.0	72	7.9	1578	3.37	24.5	712	5.3
2425	2.89	28.0	72	8.5	1714	3.41	23.7	40	6.2
					1774	3.31	31.0	363	6.2
996	3.56	7.0	138	4.5	1988	2.11	11.9	155	6.4
1013	3.59	4.6	137	3.8					
1023	3.60	6.9	138	4.0	983	7.10	7.0	138	4.6
1101	3.69	3.2	137	3.8	993	7.13	6.5	138	4.5
1113	3.70	5.3	138	4.2	1059	7.25	5.8	138	4.0
1151	3.73	8.5	136	3.6	1119	7.41	6.4	138	3.9
1217	3.80	12.5	138	4.1	1153	7.48	6.5	138	4.8
1314	3.88	4.0	137	3.9	1646	7.19	4.0	185	5.5
1413	3.95	6.3	136	4.0	1760	7.43	7.4	138	5.7
1416	3.94	4.6	137	4.7	1805	7.50	3.9	137	5.9
1576	4.05	6.3	136	4.7					
1688	3.41	16.4	131	5.2	1713	14.7	5.0	138	5.4
					1735	14.8	5.0	138	5.5

$3.43 \times 10^{-6} \text{ mol/cm}^3$ with initial mole fractions of $x(\text{NCN}_3) = 21 \text{ ppm}$ and $x(\text{C}_2\text{H}_5\text{I}) = 72 \text{ ppm}$. After the arrival of the incident shock wave, the NCN signal increases within $20 \mu\text{s}$. Obviously, both the thermal decomposition of NCN_3 and the singlet-triplet relaxation of NCN are fast. The subsequent NCN decay is well resolved and is more or less complete at the end of the experimental time window set by the Schlieren signal of the reflected shock wave at $t = 460 \mu\text{s}$.

In order to extract rate constants for reaction (2), $\text{NCN} + \text{H} \rightarrow$ products, the NCN profiles were numerically simulated using the CHEMKIN-II package.⁴⁸ The GRI-Mech 3.0 was used as a base mechanism⁴² supplemented by an iodine submechanism adopted from our previous work⁴³ and the reactions outlined in Table 1. The mechanism for NCN secondary chemistry was assembled from literature data, in particular from our previous measurements that have been validated to reproduce NCN concentration-time profiles of pure $\text{NCN}_3/\text{argon}$ mixtures over a wide range of experimental conditions. The ethyl iodide decomposition has been modeled by including the recently optimized submechanism reported by Varga et al.³⁹ (vide supra). In order to identify potential contributions of ^1NCN secondary chemistry, all triplet NCN reactions have been duplicated for singlet NCN. Although this treatment neglects the presumably different ^1NCN reactivity, it can be safely assumed that ^1NCN secondary chemistry is dominated by its relaxation reaction forming triplet NCN within the first few μs of the experiments. Thermodynamic data were taken from Burcat's thermodynamic database⁴⁹ with updated NASA polynomial parameters for NCN from Goos et al.²² Note that the assumed value for the enthalpy of formation of NCN, although of utmost importance for the discussion of the branching ratio of reaction (2) (vide infra), is not important for the determination of the total rate constant from the experimental profiles.

The solid curve in Fig. 3a reflects the best fit of the data using k_2 as an adjustable parameter. Two additional simulations using k_2 varied by a factor of two (dashed curves) are shown as well. They deviate strongly from the experimental profile demonstrating the high sensitivity of reaction (2). Assuming either the products of reaction channel (2a), $\text{CH} + \text{N}_2$, or reaction channel (2b), $\text{HCN} + \text{N}$, did not change the extracted k_2 value within error limits. The high sensitivity of reaction (2) is further outlined in the sensitivity analysis shown in Fig. 3b. Here, the sensitivity coefficient $\sigma(i, t)$ for reaction i at time t was normalized with respect to the maximum concentration $[\text{NCN}]_{\text{max}}$ over the time history, $\sigma(i, t) = 1/[\text{NCN}]_{\text{max}} \times (\partial[\text{NCN}]/\partial \ln k_i)$. For the analysis, a branching ratio of $\phi = k_{2b}/k_2 = 0.5$ has been assumed. Following the initial increase of the signal, which is determined by the NCN relaxation reaction (4), reaction (2) dominates the NCN decay. The relatively high sensitivity coefficients for reactions (5a) and (5b) directly reflect the influence of the branching ratio of reaction (5) and hence the assumed H atom yield from ethyl iodide pyrolysis. Presuming that this branching ratio is accurate, the sensitivity analysis reveals that the rate constant of reaction (2) could be directly measured under nearly pseudo first-order conditions.

Whereas the highest feasible experimental temperature was limited by the increasingly fast thermal decomposition of NCN, towards lower temperatures non-NCN secondary chemistry becomes significant as well. This is illustrated by the $T = 1150 \text{ K}$

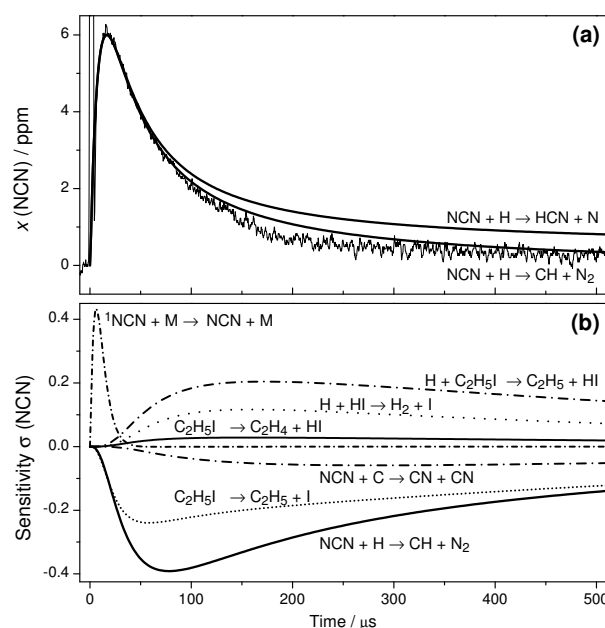


Fig. 4 (a) Experimental NCN profile in comparison with numerical simulations. $T = 1150 \text{ K}$, $\rho = 7.48 \times 10^{-6} \text{ mol/cm}^3$, $p = 720 \text{ mbar}$, $x(\text{NCN}_3) = 6.5 \text{ ppm}$, $x(\text{C}_2\text{H}_5\text{I}) = 138 \text{ ppm}$, $k_2 = 4.8 \times 10^{13} \text{ cm}^3 \text{ mol}^{-1} \text{ s}^{-1}$. (b) Sensitivity analysis.

experiment and sensitivity analysis shown in Fig. 4. Both reaction (14), $\text{H} + \text{C}_2\text{H}_5\text{I}$, and the assumed products of reaction (2) become important. Assuming the products of channel (2a), $\text{HCN} + \text{N}$, at longer reaction times the reaction $\text{N} + \text{NCN}$ significantly consumes NCN. Similarly, assuming the products of channel (2b), $\text{CH} + \text{N}_2$, the reaction $\text{C} + \text{NCN}$ gains importance. Here, C atoms are efficiently generated by the reaction $\text{CH} + \text{H} \rightarrow \text{C} + \text{H}_2$. Consistent with the expected diminishing role of the activation controlled channel (2b), somewhat better agreement with the experiment is obtained by assuming channel (2a). However, as the remaining differences between simulation and experiment could not be clearly attributed to a specific secondary reaction, no attempt was made to further improve the simulation at longer reaction times. Instead, the rate of reaction (2) was extracted from the NCN decay by fitting the transient at short reaction times where secondary chemistry did not yet exert a significant influence.

All measured rate constants k_2 are listed in Table 2 and are shown in Arrhenius form in Fig. 5. Overall, the rate constants follow the same trend independent of total density (varied by a factor of 4) and mixture composition (varied within $1.7 < [\text{C}_2\text{H}_5\text{I}]_0/[\text{NCN}_3]_0 < 60$). The data reveal a shallow minimum at temperatures around 1050-1200 K indicating that at least two reaction channels are active, presumably channels (2a) and (2b) with (2b) becoming more important towards higher temperatures. Accordingly, in the temperature range $962 \text{ K} < T < 2425 \text{ K}$ the total rate constant can be best represented by the sum of two Ar-

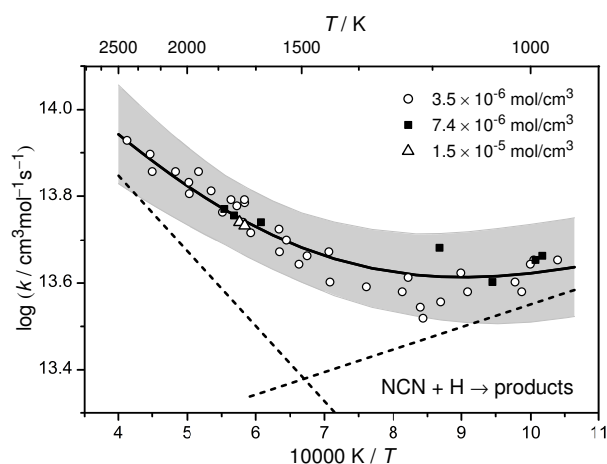


Fig. 5 Arrhenius plot for k_2 measured at three different total densities. The solid curve corresponds to a fit of the data using a sum of two Arrhenius expressions (dashed lines). The gray area represents the uncertainty range based on a comprehensive error analysis.

Arrhenius expressions,

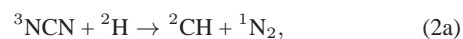
$$k_2 / (\text{cm}^3 \text{mol}^{-1} \text{s}^{-1}) = 3.49 \times 10^{14} \exp(-33.3 \text{ kJ mol}^{-1} / RT) + 1.07 \times 10^{13} \exp(+10.0 \text{ kJ mol}^{-1} / RT), \quad (1)$$

depicted as the solid curve in Fig. 5. The two single Arrhenius terms are also shown as dashed lines and can be roughly interpreted to represent the contributions of channel (2b) (first term) and channel (2a) (second term). A more refined analysis of the overall rate constant will be presented below.

An error analysis has to take into account uncertainties resulting from the scatter of the data ($\pm 6\%$), the mixture composition (in particular the initial ethyl iodide mole fraction, $\pm 3\%$), the channel branching ratio of the ethyl iodide decomposition (estimated from Fig. 2 to be $\pm 7\%$), the NCN absorption cross section ($\pm 25\%$, resulting in a 3% uncertainty in k_2), and the secondary chemistry. In the middle of the investigated temperature range ($T \approx 1600$ K), a direct pseudo first-order evaluation was possible and hence errors from secondary chemistry are minor. Nevertheless, we allow for a 10% error due to a possibly large uncertainty of the rate constant of the reaction (10), $\text{NCN} + \text{N}$, which has not been directly measured so far. Increasing its rate constant from $1 \times 10^{13} \text{ cm}^3 \text{mol}^{-1} \text{s}^{-1}$ to $1 \times 10^{14} \text{ cm}^3 \text{mol}^{-1} \text{s}^{-1}$ would make this reaction sensitive because N atoms are formed in reaction (2b) and hence slightly too high k_2 values would have been determined by our analysis. Taking into account partial error compensation, we estimate the overall uncertainty of k_2 to be $\pm 20\%$ at $T = 1600$ K, increasing to $\pm 30\%$ due to higher uncertainties resulting from secondary chemistry and the employed ethyl iodide branching ratio at the high and low temperature limit of the experiments. A corresponding uncertainty range is indicated by the grey shaded area in Fig. 5.

4 Discussion

The obtained total rate constant expression for k_2 is compared with selected literature values and further analyzed in order to derive a consistent set of rate constants for the two main high-temperature reaction channels (2a) and (2b) as well as the NCN enthalpy of formation $\Delta_f H_{298 \text{ K}}^\circ$ (ΔH in the following) in Fig. 6. As it was shown by the high level *ab initio* calculations of Teng et al.,⁴ from the four feasible reaction channels



reaction channel (2c) yielding $\text{HNC} + \text{N}$ exhibits high activation barriers and does not play a role. The recombination channel (2d), which dominates at room temperature and very high pressures, becomes less important with increasing temperature and can be expected to be of minor importance at combustion relevant temperatures $T > 1000$ K as well. At a typical total pressure of $p = 0.5$ bar used in this work, the theoretical predictions of Teng et al.⁴ range channel (2d) to contribute about 1.2% at 1000 K and 3.8% at $T = 800$ K to the overall reaction. Due to the inconsistencies in that paper (vide infra) these numbers should be interpreted with caution, however, the order of magnitude reveals that this channel starts to play a role at the lowest experimental temperatures of this study. Nevertheless, as a good starting point, we limit our analysis of the k_2 data to channels (2a) and (2b) in the following. Regarding the potential energy surface for reaction (2) from Teng et al.,⁴ channel (2a) proceeds on the doublet surface over the formation of an HNCN complex and is supposed to have a slightly negative temperature dependence. In contrast, channel (2b) exhibits a small activation barrier and predominantly proceeds on a quartet surface. The kinetic calculations also reveal that both reaction channels are important at combustion temperatures.

Analysis method a: In Fig. 6a, the upper dotted curve depicts the calculated rate expression for k_{2a} from Teng et al.⁴ The very high rate constant values for k_{2a} as well as the very high total rate constants k_2 (dashed curve included in Fig. 1) are unreasonable. Compared to our experimentally determined total rate constant values, the expression yields up to 6 times higher rate constants for channel (2a) already. Moreover, there seems to be an inconsistency in the reported rate constants for the equilibrium $\text{CH} + \text{N}_2 \rightleftharpoons \text{NCN} + \text{H}$ in the paper of Teng et al. Using their values for the rate constant of the forward reaction (1a) and their preferred value for the enthalpy of formation, $\Delta H = 458$ kJ/mol, we calculate reverse rate constants k_{2b} . Thermodynamic data for CH, N_2 , H, and NCN were taken from Burcat's database⁴⁹ with updated heat capacity data for NCN from Goos et al.,²² where 7-term NASA polynomial parameter a_6 has been scaled to adjust $\Delta H(\text{NCN})$. Obtained k_{2b} values are 2-3 times lower than reported by Teng et al. (lower dotted curve in Fig. 6a). Another indication that the reported rate constants may be flawed comes from the reported total rate constant values; for example, the recommended room temperature value $k_2 \approx 7 \times 10^{14} \text{ cm}^3 \text{mol}^{-1} \text{s}^{-1}$ is higher than the Lennard-Jones

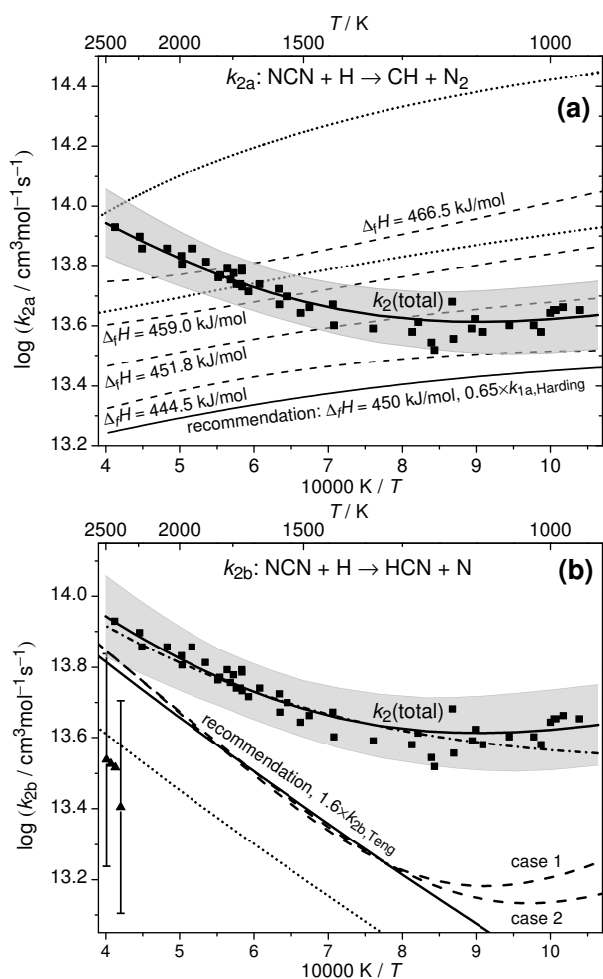


Fig. 6 Analysis of total rate constant data in terms of $\Delta_f H_{298\text{K}}^\circ(\text{NCN})$ (ΔH in the following). The squares, the corresponding solid curves, and the shaded areas reflect the experimental data for k_2 of this work and their uncertainty limits. *Upper plot a*: Analysis with respect to channel (2a). The upper dotted curve depicts the original expression for k_{2a} adopted from Teng et al.,⁴ the lower dotted curve a re-evaluation of their data using $\Delta H = 458$ kJ/mol. The dashed curves reflect $k_{2a} = k_{1a}/K$ with k_{1a} from Harding et al.³ derived for different ΔH values using Eq. (II). For the lower solid curve, Eq. (II) was scaled by a factor of 0.65. *Lower plot b*: Analysis with respect to channel (2b). Triangles with error bars and the dotted line reflect the experimental and theoretical data reported by Vasudevan et al.⁶ and Teng et al.,⁴ respectively. The dashed curves depict $k_{2b} = k_2 - k_{2a}$ expressions obtained from the k_2 values of this work and k_{2a} derived from Harding et al.; case 1: $k_2 \times 1.0$, $k_{1a} \times 1.0$, $\Delta H = 440$ kJ/mol; case 2: $k_2 \times 1.0$, $k_{1a} \times 0.65$, $\Delta H = 450$ kJ/mol. The lower solid curve reflects the recommended k_{2b} expression, which is equal to the Teng et al.⁴ expression scaled by a factor of 1.6. The dash-dotted curve corresponds to $k_2 = k_{2a} + k_{2b}$ using the two recommended rate expressions.

collision limit of $k_{LJ} \approx (3.5 - 5.5) \times 10^{14} \text{ cm}^3 \text{ mol}^{-1} \text{ s}^{-1}$, which can be estimated based on the Lennard Jones parameters reported in the literature (parameters for H: $^{50-52} \sigma = (2.00 - 3.26) \text{ \AA}$ and $\epsilon/k_B = (2.7 - 145) \text{ K}$; parameters for NCN: $^{50} \sigma = 3.83 \text{ \AA}$ and $\epsilon/k_B = 232 \text{ K}$).

To the best of our knowledge, no other experimental or theoretical values for k_{2a} have been reported explicitly in the literature yet. Therefore, we continue our analysis by calculating k_{2a} values from the reverse reaction k_{1a} , which has been thoroughly studied both experimentally and theoretically. For an overview of available literature data we refer to the work of Harding et al.³ who performed high-level *ab initio* and transition state theory calculations on the reaction $\text{CH} + \text{N}_2$ using multi-reference electronic structure methods. Using their recommended value of the enthalpy of formation, $\Delta H = 459$ kJ/mol, the theoretical prediction was found to be in quantitative agreement with the most recent shock tube data of Vasudevan et al.⁶ over the temperature range $2100 \text{ K} < T < 3350 \text{ K}$. At these high temperatures, the predicted rate constant is less dependent on the assumed value of ΔH . Towards lower temperatures and in the practically important temperature range of $1000 - 2000 \text{ K}$, however, an accurate enthalpy of formation is crucial. In an Arrhenius plot, Harding et al.³ present their results of temperature dependent calculations of the rate constant of reaction (1a) assuming different values for the enthalpy of formation of NCN (Fig. 13 in their paper). For example, it was shown that changing ΔH by ± 8 kJ/mol yields a factor of 1.6 higher (-8 kJ/mol) or 1.9 lower ($+8$ kJ/mol) k_{1a} value at $T = 1000 \text{ K}$. In order to take this pronounced thermodynamic effect into account in our analysis and to derive rate constant estimates for $k_{2a} = k_{1a}/K$ as function of the assumed NCN enthalpy of formation, we reparametrized the original data of Harding et al. and used the expression

$$k_{1a}/(\text{cm}^3 \text{ mol}^{-1} \text{ s}^{-1}) = e^{(274.5 - 0.556x)} \times (T/\text{K})^{(-31.24 + 0.0706x)} \times e^{(-71.2 \text{ kJ mol}^{-1}/RT)} \quad (\text{II})$$

with $x = \Delta_f H_{298\text{K}}^\circ(\text{NCN})$ in kJ/mol. Eq. (II) provides a stable fit of the rate constant data of Harding et al. and yields a reasonable extrapolation to somewhat higher and lower $\Delta_f H_{298\text{K}}^\circ(\text{NCN})$ values. Representative literature values of the enthalpy of formation span the range from 444.5 kJ/mol (single-reference computations)^{16,23} to 459 kJ/mol (high-level basis set extrapolation or multi-reference computations)^{3,4} for theoretical and from 451.8 kJ/mol (electron affinity of NCN)⁵³ to 466.5 kJ/mol (NCN photodissociation)²⁴ for experimental literature data. The resulting k_{2a} expressions are shown as dashed curves in Fig. 6a. They reveal a weak and negative temperature dependence of the reaction $\text{NCN} + \text{H} \rightarrow \text{CH} + \text{N}_2$ with the absolute rate constant values basically offset by the assumed enthalpy of formation of NCN. Clearly, the higher enthalpies of formation yield unfeasible k_{2a} values that are up to a factor of 2.4 higher than the total rate constant measured in this work. Assuming that (i) the branching fraction $k_{2a}/k_2 = 1$ around $T = 1000 \text{ K}$, (ii) k_{1a} from Harding et al. is correct, and (iii) k_2 is at the upper limit of the uncertainty range of our experimental data ($+30\%$), an upper limit of $\Delta H < 454$ kJ/mol can be estimated from this analysis.

Analysis method b: A second analysis of our data focusing on

the rate constant of channel (2b) is shown in Fig. 6b. The indirect experimental data of Vasudevan et al.⁶ (triangles with error bars) and the most recent theoretical estimate of Teng et al.⁴ (dotted curve) are shown as well. In the light of the negative temperature dependence of channel (2a) it becomes clear that the experimentally determined positive temperature dependence of k_2 towards higher temperatures arises from the increasingly dominant activation controlled channel (2b). Moreover, the high temperature activation energy $E_a = 33$ kJ/mol estimated from the two channel fit of our experimental data (see Fig. 5 and Eq. (I)) is in very good agreement with the theoretically predicted activation energies of 35 kJ/mol and 28 kJ/mol reported by the M.C. Lin group^{2,4} (see Figs. 1 and 6b). Hence, we consider the activation energy of reaction channel (2b) a well-constrained quantity with a preferred value of $E_a \approx 28$ kJ/mol adopted from the most recent *ab initio* study.⁴ Having the temperature dependence of k_{2b} fixed, it is possible to arrive at a consistent value for the enthalpy of formation. Here, ΔH has been chosen in a way such that the rate constant expression for $k_{2b} = k_2 - k_{2a}$, with k_2 values taken from Eq. (I) of this work and k_{2a} values calculated via thermodynamic equilibrium from the k_{1a} expression Eq. (II), yields a temperature dependence that is consistent with 28 kJ/mol. A matrix of appropriate enthalpy of formations with k_2 and k_{1a} varied within their uncertainty limits is given in Table 3. Here, uncertainties of $k_2 \pm 30\%$ as obtained in this work and $k_{1a} \pm 35\%$ as reported for the experimental shock tube results of Vasudevan et al.⁶ (which are in turn consistent with the k_{1a} expression of Harding et al.) have been assumed. Table 3 reveals a large range of possible enthalpy of formations, 423 kJ/mol $< \Delta H < 456$ kJ/mol. Nevertheless, two conclusions can be drawn from this analysis. First, increasing k_{1a} yields unfeasible enthalpy values that are even well below the results of the single-reference computations (about 444.5 kJ/mol), which can be regarded a reasonable lower limit for ΔH . Even with k_{1a} unchanged, the highest value of 445 kJ/mol would be close to this limit. Secondly, the upper limit of 456 kJ/mol, corresponding to a scenario with $k_2 + 30\%$ and $k_{1a} - 35\%$, is in agreement with the upper limit of 454 kJ/mol inferred from analysis method a. Therefore, the high experimental value of Bise et al.²⁴ (466.5 ± 2.9 kJ/mol), the results of the high-level basis set extrapolation and multi-reference computations (about 459 kJ/mol),^{3,4} and the most recent recommendation of the Active Thermochemical Tables as cited in Goos et al.²² (457.8 ± 2) are hardly compatible with this work.

Resulting k_{2b} expressions are illustrated in Fig. 6b for two selected cases. Case 1, assuming that both k_2 and k_{1a} exhibit values as given by Eqs. (I) and (II), yields $\Delta H = 440$ kJ/mol. Case 2, assuming k_2 from Eq. (I) and k_{1a} from Eq. (II) scaled by a factor of 0.65, yields $\Delta H = 450$ kJ/mol. For all other cases outlined in Table 3, similar k_{2b} curves have been obtained, of course somewhat offset for different assumed k_{1a} values (not shown). It is obvious from Fig. 6b that the calculated k_{2b} expressions deviate from linearity at temperatures below 1250 K. With decreasing temperatures and hence a decreasing contribution of k_{2b} the analysis procedure gets less reliable, hence, part of this deviation may be attributed to inaccuracies of the analysis method itself. However, it may also indicate the onset of the low temperature reaction channel (2d), which has been neglected in the analysis. In this sense, the increase of k_{2b} at low temperatures would simply

Table 3 Feasible values of $\Delta_f H_{298\text{K}}^\circ(\text{NCN})$ for different combinations of k_{1a} and k_2 values. The reported enthalpy values in kJ/mol yield activation energies $E_{a,2a} \approx 28$ kJ/mol for reaction channel (2a) that are consistent with the corresponding theoretical estimate of Teng et al.⁴

$\Delta_f H_{298\text{K}}^\circ(\text{NCN})$	$k_2 + 30\%$	k_2	$k_2 - 30\%$
$k_{1a} + 35\%$	436	430	423
k_{1a}	445	440	432
$k_{1a} - 35\%$	456	450	443

arise from the neglected contributions of this channel.

Overall, relying on the direct k_2 determination of this work, an enthalpy value of 450 kJ/mol is most consistent with both the enthalpy limits set by the single-reference computations and our analysis, $444.5 \text{ kJ/mol} < \Delta_f H_{298\text{K}}^\circ(\text{NCN}) < 454 \text{ kJ/mol}$, the experimental and theoretical values for k_{1a} from Vasudevan et al.⁶ and Harding et al.,³ the activation energy of reaction channel (2b) reported by Teng et al.,⁴ and the indirect shock tube measurements for k_{2b} from Vasudevan et al.⁶ This enthalpy value is also in very good agreement with the experimental electron affinity measurements of Clifford et al.⁵³ (451.8 ± 16.7 kJ/mol) that has been, for example, used in the GDFkin3.0_NCN flame modelling mechanism as well.⁸

Using $\Delta H = 450$ kJ/mol, the recommended rate constant expressions for k_{1a} , k_{2a} , and k_{2b} are as follows: Compatible with the lower experimental uncertainty limit of Vasudevan et al., k_{1a} is set to 0.65 times the values of Harding et al. (Eq. (II)):

$$k_{1a}/(\text{cm}^3 \text{mol}^{-1} \text{s}^{-1}) = 2.3 \times 10^{10} \times (T/\text{K})^{0.53} \times \exp(-71.2 \text{ kJ/mol}/RT)$$

Using the updated NASA polynomial parameters for NCN from Goos et al.²² (scaled to $\Delta H = 450$ kJ/mol), this corresponds to a reverse reaction rate constant k_{2a} of

$$k_{2a}/(\text{cm}^3 \text{mol}^{-1} \text{s}^{-1}) = 4.2 \times 10^{15} \times (T/\text{K})^{-0.69} \times \exp(-2.0 \text{ kJ/mol}/RT)$$

Adopting the temperature dependence of Teng et al., their rate expression is recommended for k_{2b} adjusted by a factor of 1.6 to fit the case 2 data in Fig. 6b:

$$k_{2b}/(\text{cm}^3 \text{mol}^{-1} \text{s}^{-1}) = 7.94 \times 10^{12} \times (T/\text{K})^{0.41} \times \exp(-22.8 \text{ kJ/mol}/RT)$$

This expression is also compatible with the upper limit of the indirect shock tube measurements of Vasudevan et al.⁶

Finally, the sum of k_{2a} and k_{2b} is shown in Fig. 6b as dash-dotted curve. It is in close agreement with the k_2 rate expression given by Eq. (I), except at the lowest temperatures where channel k_{2d} presumably starts to play a role. The recommended rate expression for k_{2b} corresponds to a branching ratio $\phi = k_{2b}/k_2$ that increases from $\phi = 0.21$ at $T = 1000$ K to $\phi = 0.74$ at $T = 2500$ K. Hence, in the temperature range relevant for flame modelling, channel switching between channel (2a) dominating at low temperatures and channel (2b) dominating at high temperatures takes place.

5 Concluding Remarks

The overall rate constant of the reaction $\text{NCN} + \text{H}$ has been directly measured at temperatures between 962 K and 2425 K behind shock waves using the thermal decomposition of NCN_3 and $\text{C}_2\text{H}_5\text{I}$ as suitable precursors for NCN radicals and H atoms, respectively. A conservative error analysis revealed that comparatively narrow error limits of $\pm 20\%$ at $T = 1600$ K, increasing to $\pm 30\%$ at the upper and lower temperature limits of the measurements, could be achieved. A main error arises from the possibly large uncertainty of the potentially important secondary reaction (10), $\text{NCN} + \text{N}$, which has not been measured yet. If the theoretical estimate of Moskaleva and Lin² turns out to be right, the influence of reaction (10) would be very small and the error estimate could be further reduced. The second most important uncertainty is related to the assumed overall H atom yield from $\text{C}_2\text{H}_5\text{I}$ decomposition. However, relying on the very recently published global analysis data on the ethyl iodide composition by Varga et al.,³⁹ this error contribution could be safely assumed to be not more than 7% (an error estimate of 3.5% at $T = 1200$ K has been stated in the original paper).

The high reliability of the rate constant data enabled us to analyze the k_2 data in terms of branching ratio and the crucial value of the enthalpy of formation of NCN . Taking into account experimental and theoretical literature data for the rate constant of reaction (1a) and the temperature dependence of reaction channel (2b), $\Delta_f H_{298\text{K}}^\circ = 450$ kJ/mol was found to be most consistent. With a robust upper limit of $\Delta_f H_{298\text{K}}^\circ < 456$ kJ/mol derived from the k_2 values of this work, significantly higher literature values – about 459 kJ/mol from high-level *ab initio* calculations^{3,4} and 466.5 kJ/mol from NCN photodissociation experiments²⁴ – are at odds with our analysis. Clearly, more work is needed to further constrain the uncertainty of the enthalpy of formation of NCN .

Modelling of NO_x formation in flames critically depends on the branching ratio of the reaction $\text{NCN} + \text{H}$. Whereas channel (2a) constitutes the reverse reaction of the main prompt- NO formation reaction (1a), $\text{CH} + \text{N}_2$, it is in particular reaction channel (2b) with the products $\text{HCN} + \text{N}$ that brings the overall reaction forward on the prompt- NO pathway. The results of this study with branching fractions $\phi = k_{2b}/k_2$ increasing from $\phi(T = 1000\text{K}) = 0.21$ to $\phi(T = 2500\text{K}) = 0.74$ verifies the expected strong temperature dependence of this quantity. However, again the actual value of the derived branching ratio strongly depends on the assumed value of the enthalpy of formation of NCN . In fact, accurate measurements of the branching ratio would be very useful to constrain the enthalpy of formation of NCN . Moreover, in conjunction with the already compiled theoretical and experimental rate constant data, accurate branching fractions would help to draw final conclusions on this reaction system including the contributions of the recombination channel (2d), which may play a role even at temperatures as high as 1000 K.

Acknowledgements

We would like to thank the German Science Foundation (FR1529/4) for funding, M.C. Lin for sharing data prior to pub-

lication, and Friedrich Temps for continued scientific support.

References

- 1 C. P. Fenimore, *Proc. Combust. Inst.*, 1971, **13**, 373–380.
- 2 L. V. Moskaleva and M. C. Lin, *Proc. Combust. Inst.*, 2000, **28**, 2393–2401.
- 3 L. B. Harding, S. J. Klippenstein and J. A. Miller, *J. Phys. Chem. A*, 2008, **112**, 522–532.
- 4 W.-S. Teng, L. V. Moskaleva, H.-L. Chen and M. C. Lin, *J. Phys. Chem. A*, 2013, **117**, 5775–5784.
- 5 G. P. Smith, *Chem. Phys. Lett.*, 2003, **367**, 541–548.
- 6 V. Vasudevan, R. K. Hanson, C. T. Bowman, D. M. Golden and D. F. Davidson, *J. Phys. Chem. A*, 2007, **111**, 11818–11830.
- 7 A. A. Konnov, *Combust. Flame*, 2009, **156**, 2093–2105.
- 8 N. Lamoureaux, P. Desgroux, A. E. Bakali and J. Pauwels, *Combust. Flame*, 2010, **157**, 1929–1941.
- 9 R. S. Zhu and M. C. Lin, *J. Phys. Chem. A*, 2007, **111**, 6766–6771.
- 10 R. S. Zhu, M. T. Nguyen and M. C. Lin, *J. Phys. Chem. A*, 2009, **113**, 298–304.
- 11 R. S. Zhu and M. C. Lin, *Int. J. Chem. Kinet.*, 2005, **37**, 593–598.
- 12 C.-L. Huang, S. Y. Tseng, T. Y. Wang, N. S. Wang, Z. F. Xu and M. C. Lin, *J. Chem. Phys.*, 2005, **122**, 184321.
- 13 T.-J. Yang, N. S. Wang, L. C. Lee, Z. F. Xu and M. C. Lin, *J. Phys. Chem. A*, 2008, **112**, 10185–10192.
- 14 A. Busch, *PhD thesis*, Karlsruher Institut für Technologie, 2010.
- 15 A. Busch and M. Olzmann, *Shock-Tube Study of the Thermal Decomposition of NCN*, Proc. European Combust. Meeting Vienna, paper P810138, 2009.
- 16 J. Dammeier and G. Friedrichs, *J. Phys. Chem. A*, 2010, **114**, 12963–12971.
- 17 J. Dammeier, N. Faßheber and G. Friedrichs, *Phys. Chem. Chem. Phys.*, 2012, **14**, 1030–1037.
- 18 J. Dammeier and G. Friedrichs, *J. Phys. Chem. A*, 2011, **115**, 14382–14390.
- 19 J. A. Sutton, B. A. Williams and J. W. Fleming, *Combust. Flame*, 2012, **159**, 562–576.
- 20 P. Glarborg, M. U. Alzueta, K. Dam-Johansen and J. A. Miller, *Combust. Flame*, 1998, **115**, 1–27.
- 21 N. Lamoureaux, C. M. Western, X. Mercier and P. Desgroux, *Combust. Flame*, 2013, **160**, 755–765.
- 22 E. Goos, C. Sickfeld, F. Mauß, L. Seidel, B. Ruscic, A. Burcat and T. Zeuch, *Proc. Combust. Inst.*, 2013, **34**, 657–666.
- 23 S. Canneaux, A. Wallet, M. Ribaucour and F. Lousi, *Comp. Theor. Chem.*, 2011, **967**, 67–74.
- 24 R. T. Bise, A. A. Hoops and D. M. Neumark, *J. Chem. Phys.*, 2001, **114**, 9000–9011.
- 25 M. Colberg and G. Friedrichs, *J. Phys. Chem. A*, 2006, **110**, 160–170.
- 26 H. Bock and R. Dammel, *Angew. Chem. Int. Ed.*, 1987, **26**, 504–526.
- 27 D. J. Benard, C. Linnen, A. Harker, H. H. Michels, J. B. Addison and R. Ondercin, *J. Phys. Chem. B*, 1998, **102**, 6010–6019.
- 28 J. Dammeier, B. Oden and G. Friedrichs, *Z. Phys. Chem.*, 2012, **45**, 30–40.
- 29 D. E. Milligan, M. E. Jacox and A. M. Bass, *J. Chem. Phys.*, 1965, **43**, 3149–3160.
- 30 J. Dammeier, *PhD thesis*, Universität Kiel, 2011.
- 31 S. S. Kumaran, M.-C. Su, K. P. Lim and J. V. Michael, *Proc. Combust. Inst.*, 1996, **26**, 605–611.
- 32 Y. Yamamori, K. Takahashi and T. Inomata, *J. Phys. Chem. A*, 1999, **103**, 8803–8811.
- 33 A. Miyoshi, N. Yamauchi, K. Kosaka and M. Koshi, *J. Phys. Chem. A*, 1999, **103**, 46–53.

- 34 J. Herzler and P. Roth, *Phys. Chem. Chem. Phys.*, 2002, **4**, 5259–5264.
- 35 B. R. Giri, T. Bentz, H. Hippler and M. Olzmann, *Z. Phys. Chem.*, 2009, **223**, 539–549.
- 36 T. Bentz, M. Szőri, B. Viskolcz and M. Olzmann, *Z. Phys. Chem.*, 2011, **225**, 1117–1128.
- 37 X. Yang and R. S. Tranter, *Int. J. Chem. Kinet.*, 2012, **44**, 433–443.
- 38 K. H. Weber, J. M. Lemieux and J. S. Zhang, *J. Phys. Chem. A*, 2009, **113**, 583–591.
- 39 T. Varga, G. Zsély, T. Turányi, T. Bentz and M. Olzmann, *Int. J. Chem. Kinet.*, 2014.
- 40 T. Turányi, T. Nagy, G. Zsély, M. Cserhádi, T. Varga, B. T. Szabó, I. Sedyó, P. T. Kiss and H. J. C. A. Zempléni, *Int. J. Chem. Kinet.*, 2012, **44**, 284–302.
- 41 G. Friedrichs, D. F. Davidson and R. K. Hanson, *Int. J. Chem. Kinet.*, 2002, **34**, 374–386.
- 42 G. P. Smith, D. M. Golden, M. Frenklach, N. W. Moriarty, B. Eiteneer, M. Goldenberg, C. T. Bowman, R. Hanson, S. Song, W. C. Gardiner Jr., V. Lissianski and Z. Qin, *GRI-Mech Version 3.0*, 1999.
- 43 G. Friedrichs, D. F. Davidson and R. K. Hanson, *Int. J. Chem. Kinet.*, 2002, **34**, 374–386.
- 44 C. K. Westbrook, *Proc. Combust. Inst.*, 1982, **19**, 127–141.
- 45 D. L. Baulch, C. T. Bowman, C. J. Cobos, R. A. Cox, T. Just, J. A. Kerr, M. J. Pilling, D. Stocker, J. Troe, W. Tsang, R. W. Walker and J. Warnatz, *J. Phys. Chem. Ref. Data*, 2005, **34**, 757–1397.
- 46 P. Camilleri, R. M. Marshall and H. Purnell, *J. Chem. Soc.*, 1974, **70**, 1434–1444.
- 47 D. L. Baulch, C. J. Cobos, R. A. Cox, C. Esser, P. Frank, T. Just, J. A. Kerr, M. J. Pilling, J. Troe, R. W. Walker and J. Warnatz, *J. Phys. Chem. Ref. Data*, 1992, **21**, 411–429.
- 48 R. J. Kee, F. M. Rupley and J. A. Miller, *Chemkin-II: A Fortran Chemical Kinetics Package for the Analysis of Gas-Phase Chemical Kinetics*, Sandia National Laboratories Sandia Report SAND89-8009, 1989.
- 49 E. Goos, A. Burcat and B. Ruscic, *Extended Third Millennium Ideal Gas and Condensed Phase Thermochemical Database for Combustion with Updates from Active Thermochemical Tables*, 2009, <http://garfield.chem.elte.hu/Burcat/burcat.html> (last access: 22 April 2014).
- 50 R. J. Kee, F. M. Rupley, J. A. Miller, M. E. Coltrin, J. F. Grcar, E. Meeks, H. K. Moffat, A. E. Lutz, G. Dixon-Lewis, M. D. Smooke, J. Warnatz, G. H. Evans, R. S. Larson, R. E. Mitchell, L. R. Petzold, W. C. Reynolds, M. Caracotsios, W. E. Stewart, P. Glarborg, C. Wang and O. Adigun, *CHEMKIN Collection (transport database)*, Release 3.6, Reaction Design, Inc., San Diego, CA (2000).
- 51 M. Freindorf, Y. Shao, T. R. Furlani and J. Kong, *J. Comput. Chem.*, 2005, **26**, 1270–1278.
- 52 A. W. Jasper and J. A. Miller, *Combust. Flame*, 2014, **161**, 101–110.
- 53 E. P. Clifford, P. G. Wenthold, W. C. Lineberger, G. A. Petersson and G. B. Ellison, *J. Phys. Chem. A*, 1997, **101**, 4338–4345.